

Absorption instruments inter-comparison campaign at the Arctic Pallas station

Eija Asmi¹, John Backman¹, Henri Servomaa¹, Aki Virkkula¹, Maria Gini², Kostas Eleftheriadis², Thomas Müller³, Sho Ohata^{4,5}, Yutaka Kondo⁶, and Antti Hyvärinen¹

¹Finnish Meteorological Institute, Helsinki, Finland

²ERL Institute of Nuclear and Radiological Science & Technology, NCRS Demokritos, Attiki, Greece

³Leibniz Institute for Tropospheric Research e.V. (TROPOS), Leipzig, Germany

⁴Institute for Space–Earth Environmental Research, Nagoya University, Nagoya, Aichi, Japan

⁵Institute for Advanced Research, Nagoya University, Nagoya, Aichi, Japan

⁶National Institute of Polar Research, Tachikawa, Japan

Correspondence: Eija Asmi (eija.asmi@fmi.fi)

Abstract. Aerosol light absorption was measured during one month field campaign in June–July 2019 at the Pallas Global Atmospheric Watch (GAW) station in northern Finland. Very low aerosol concentrations prevailed during the campaign which imposed a challenge for the instruments detection limits. Thus, the campaign provided a real-world test for different absorption measurement techniques supporting the goals of the EMPIR BC metrology project in developing aerosol absorption standard and reference methods. In this study we compare the results from five filter-based absorption techniques: Aethalometer models AE31 and AE33, Particle Soot Absorption Photometer (PSAP), Multi Angle Absorption Photometer (MAAP) and Continuous Soot Monitoring System (COSMOS), and from one indirect technique called Extinction Minus Scattering (EMS). The ability of the filter-based techniques was shown to be adequate to measure aerosol light absorption coefficients down to around 0.01 Mm⁻¹ levels when data was averaged to 1–2 hs. The 1h-averaged atmospheric absorption that was measured using the MAAP as a reference was 0.09 Mm⁻¹ (at wavelength of 637 nm). When data was averaged for >1h, an agreement of around 15–20% was obtained between the instruments. COSMOS measured systematically the lowest absorption coefficient values, which was expected due to the sample pre-treatment in COSMOS inlet. PSAP showed the best linear correlation with MAAP (slope = 0.95, R² = 0.78), followed by AE31 (slope=0.93). However, the noisy AE31 data decreased the significance of this correlation (R² = 0.65). Statistically the best correlations with MAAP were obtained for AE33 and COSMOS, but biases at around the zero values led to slopes clearly below one. In COSMOS, also the sample pre-treatment could affect on the correlation slope. In contrast to the filter-based techniques, the sensitivity of the indirect EMS method to measure aerosol absorption was not adequate at such low concentrations levels. An absorption coefficient on the order of >0.1 Mm⁻¹ was estimated as the lowest limit, to reliably distinguish the EMS signal from the noise at 1–2 hs averaging time. The mass absorption cross-section (MAC) value was calculated using MAAP and SP2 as reference instrument, leading to a MAC value of 16.0 m² g⁻¹. The results demonstrate the challenges encountered in the absorbing aerosol measurements in pristine environments and provide some useful guidelines for instruments selection and uncertainty analysis.

1 Introduction

The development of a filter-based absorption measurement method began with an experiment by Rosen et al. (1978). The Raman spectral measurements confirmed that the light attenuation is proportional to the graphitic soot content on a filter. After
25 this discovery the development continued by Hansen et al. (1982, 1984), and today, the various filter-based techniques are commonly used in aerosol absorption measurements (Tørseth et al., 2019). The filter-based methods are sensitive, simple and robust, and therefore widely applicable.

Meanwhile, it has become evident that the filter-based methods are prone to several filter artifacts. These include the dependence of light attenuation on the filter tape loading and the interference of aerosol light scattering with the absorption
30 measurement (Müller et al., 2011). Aerosol size affects the penetration depth in a filter adding another size dependent measurement artifact (Kondo et al., 2009; Nakayama et al., 2010). Additional sources of uncertainties are the variations in filter spot size and the non-idealities of light source (Bond et al., 1999). Various algorithms to correct for these artifacts have been developed (Bond et al., 1999; Weingartner et al., 2003; Arnott et al., 2005; Schmid et al., 2006; Virkkula et al., 2007; Nakayama
35 et al., 2010; Ogren, 2010; Virkkula, 2010; Collaud Coen et al., 2010). The diverse use of these algorithms complicates a direct comparison of aerosol absorption values from different studies. The measured aerosol light absorption is frequently reported as equivalent black carbon (eBC) mass [in units: ng m^{-3}] which relies on a specific wavelength dependent mass absorption cross section (MAC) coefficient (Bond and Bergstrom, 2006; Petzold et al., 2013).

Alternative absorption measurement methods exist. They are less prone to measurement artifacts and have been used for development of algorithms to remedy the uncertainties associated with the filter-based techniques. Photoacoustic techniques
40 have the advantage to measure particle absorption in their natural atmospheric state suspended in air (Arnott et al., 1999). However, they suffer from artifacts related to the gas composition and are less robust and sensitive than the filter-based techniques. An individual particle analysis with a laser-induced incandescence (LII) technique is to date the most accurate and sensitive method to measure the absorbing mass content, the so called refractory black carbon (rBC) mass, of the aerosol. The existing LII techniques are expensive and complex, and converting the rBC signal to atmospheric absorption is not straightforward
45 (Schulz et al., 2006; Schwarz et al., 2006). A simultaneous measurement of the aerosol extinction and scattering is yet another alternative that allows to derive the aerosol absorption indirectly (Strawa et al., 2003; Virkkula et al., 2005). A review of methods with their common pros and cons is provided by Moosmüller et al. (2009).

The different methods to measure aerosol light absorption have been compared and verified in previous laboratory (Saathoff et al., 2003; Slowik et al., 2007; Müller et al., 2011) and field (Reid et al., 1998; Schmid et al., 2006; Kanaya et al., 2008;
50 Kondo et al., 2011; Backman et al., 2017; Laing et al., 2020) campaigns. The campaigns have focused on characterizing uncertainties of the different absorption techniques and examined their response to varying absorbing aerosol sources. Reid et al. (1998) measured Brazilian biomass burning aerosol using six different techniques, concluding about 20% convergence between them. Kanaya et al. (2008) found an overall good agreement between the results of different instruments, but the discrepancies increased at high Organic Carbon (OC) content. Schmid et al. (2006) measured the Amazon biomass burning
55 aerosol using various methods and estimated 15% and 20% accuracy, for PSAP and Aethalometer measurement, respectively.

Better agreement, in terms of eBC mass, can be expected when solely non-volatile absorbing particle is analyzed avoiding any artifacts from volatile light scattering particles (Kondo et al., 2011).

Accuracy of the aerosol absorption measurement methods needs to be improved to reduce the uncertainties associated with their climate impacts. Absorbing aerosol has an accelerating impact on the global temperature rise, which is further intensified over the Polar Regions due to the regional strong climate feedbacks. The aerosol light absorption, and its spatial and temporal variability, are therefore of specific concern in the Arctic. Absorption measurements in the Arctic require sensitive and robust techniques. While previous work has presented data analysis techniques aimed to improve the detection capabilities of the absorption instruments (Springston et al., 2007; Hagler et al., 2011; Backman et al., 2017), comprehensive absorption instrument characterizations at pristine locations are lacking. Recently, Backman et al. (2017); Schmeisser et al. (2018) found significant spatial differences in aerosol light absorption seasonal characteristics in the Arctic. All long-term aerosol absorption data series from the Arctic are measured using filter-based methods. Backman et al. (2017) used the co-located measurements to construct a homogeneous dataset for multiple Arctic sites, but the instruments were never applied all in parallel. Such a parallel comparison in the Arctic would assist to estimate the uncertainties associated to these measurements.

The EMPIR BC project develops metrology for light absorption by atmospheric aerosols. It aims at finding standard reference materials that mimic atmospheric absorbing aerosol and a traceable, primary method to determine the aerosol absorption coefficients. An additional goal of the EMPIR BC project is to develop a validated transfer standard for field calibrations. The Pallas campaign was the first field campaign in the project. The goal was to test the stability, accuracy and detection capabilities of the commonly available absorption measurement methods focusing on the filter-based techniques, and to conclude on their applicability in pristine environments. To our knowledge, this is the most comprehensive absorption and BC mass measurement instrument parallel field comparison done in the Arctic.

2 Methodology

2.1 The Pallas site description

The Pallas atmosphere ecosystem supersite is located in the northern Finland inside the Arctic. It is part of the Pallas-Sodankylä Global Atmospheric Watch (GAW) station and contributes to various national and international networks and programmes. Important in this context is the Aerosols, Clouds, and Trace gases Research InfraStructure (ACTRIS) to which Pallas provides quality controlled and continuous data on aerosol number, size and optical properties. The main station for aerosol measurements at Pallas is on top of the Sammaltunturi fell ($67^{\circ} 58' N$, $24^{\circ} 07' E$, 560 m a.g.l.) where also the EMPIR BC field campaign was organized. A detailed description of the site, its surroundings and on-going measurement programmes were published earlier by Hatakka et al. (2003); Lohila et al. (2015).

The EMPIR BC field campaign took place during the Nordic summer, between 19.6 – 17.7.2019. A summary of the instrumentation used with corresponding settings during the campaign are presented in Table 1. Each instruments operational principle and respective data corrections are presented in detail below.

2.2 Aerosol optical properties

Table A1 summarizes the quantities that frequently appear in this manuscript text. All the filter-based instruments target to achieve aerosol light absorption coefficients $\sigma_{AP,\lambda}$ at instrument specific wavelengths λ , which are acquired from the measured light attenuation using signal post-processing. $\sigma_{AP,\lambda}$ is a measure of the absolute magnitude of atmospheric absorption, or the cross-section of light-absorbing material (BC) available in a volume of air in which this material exists. This cross-section can be normalized to particle mass by a simple factor called mass absorption cross-section (MAC) (Bond and Bergstrom, 2006). Some applications, such as atmospheric modeling, favor the use of BC mass over the absorption coefficient, for which the value of MAC needs to be known.

Here, when referring to a corrected absorption coefficient measured using a particular technique, a notation $\sigma_{INST,\lambda}$, where INST is an abbreviation of the technique, is used. When referring to an aerosol light absorption coefficient value directly reported by the instrument, $\sigma_{0,\lambda}$ is used instead.

A typical measure of aerosol "brightness" is the ratio of aerosol scattering $\sigma_{SP,\lambda}$ to aerosol extinction $\sigma_{EP,\lambda}$, a parameter called single-scattering albedo

$$\omega_{0,\lambda} = \frac{\sigma_{SP,\lambda}}{\sigma_{EP,\lambda}} = \frac{\sigma_{SP,\lambda}}{\sigma_{SP,\lambda} + \sigma_{AP,\lambda}}, \quad (1)$$

which is of great significance when assessing the radiative forcing of the aerosols. The scattering wavelength dependence is described as

$$\sigma_{SP,\lambda_1} / \sigma_{SP,\lambda_2} = (\lambda_1 / \lambda_2)^{-\alpha_{SP,\lambda}}, \quad (2)$$

where $\alpha_{SP,\lambda}$ is called the Ångström exponent of scattering and is related with the aerosol optical size. A similar wavelength dependent parameter, $\alpha_{AP,\lambda}$, can be defined for aerosol absorption.

Interpolation of $\sigma_{SP,\lambda}$ to any wavelength λ was done by applying the calculated Ångström exponent at the nearest available wavelengths (Anderson and Ogren, 1998). Interpolation of $\sigma_{AP,\lambda}$ to a wavelength λ was done by assuming a simple relation between the wavelengths and variation in $\alpha_{AP,\lambda}$ was not accounted for due to high noise in data.

2.3 Instruments

Data from five filter-based absorption photometers, two instruments that measure aerosol scattering, two instruments that measure aerosol extinction and one instrument that measure refractory BC are used in this paper. The data were corrected with the best practices considered for each particular instrument independently, following the global guidelines, literature citations and earlier work done at the station.

The flow rate of each instrument was measured at the beginning and at the end of the campaign with a Gilian flow calibrator (volumetric flow rate), and converted to standard (STP) conditions (0°C, 1013hPa) after which the flow correction based on the equation 5 in Bond et al. (1999) was applied. Instrument flow rates are shown in Table 1.

2.3.1 AE31

120 Aethalometer model AE31 (Magee Scientific Inc.) is part of the permanent installation at Pallas site since year 2005 (Li-havainen et al., 2015). It measures the aerosol absorption coefficient at seven wavelengths: 370 nm, 470 nm, 520 nm, 590 nm, 660 nm, 880 nm and 950 nm. The measurement principle is based on the observed light attenuation caused by the particles that are continuously collected on a filter tape (Hansen et al., 1982, 1984). The aerosol attenuation coefficient is then calculated as

$$\sigma_{0,\lambda} = \frac{A}{Q * 100} * \frac{\Delta ATN}{\Delta t}, \quad (3)$$

125 where A is the filter spot size, Q is the flow rate and ΔATN is the measured change in the attenuation during the time interval Δt . AE31 changed the filter spot automatically when a pre-set limit value of $ATN = 60$ was reached. The instrument reports data in eBC mass concentration which is simply the measured aerosol absorption coefficient corrected with a wavelength dependent specific attenuation.

130 The AE31 data measured at Pallas was corrected for the multiple scattering of light by filter fibers by dividing $\sigma_{0,\lambda}$ with a multiple scattering enhancement factor, $C_0 = 3.5$, which is selected according to the global recommendation of the Global Atmospheric Watch's World Calibrations Centre for Aerosol Physics (GAWReport No. 227; <http://wmo-gaw-wcc-aerosol-physics.org/wmo-gaw-reports.html>), and is also very close to the C_0 factor for the Arctic given by Backman et al. (2017). The filter loading artifact was corrected using the method by Virkkula et al. (2007, 2015), and the Pallas station specific correction factor $k = 0.0038$ (Backman et al., 2017). Note that this correction is a loading correction only, unlike the algorithms of Arnott et al. (2005) and Collaud Coen et al. (2010) in which a fraction of scattering coefficient is subtracted from $\sigma_{0,\lambda}$.

135 2.3.2 AE33

An updated version of the AE31 is the dual-spot aethalometer model AE33 (Drinovec et al., 2015). The instrument reports an aerosol light absorption coefficient based on the measured attenuation on two parallel filter spots with different particle loadings. It applies a real-time loading effect compensation algorithm that is essentially based on the work by Virkkula et al. (2007). The Pallas AE33 uses an internal multiple scattering correction factor $C_0 = 1.39$ (Drinovec et al., 2015). This was 140 corrected to a value $C_0 = 3.5$ in order to comply with the global recommendation (GAWReport No. 227; <http://wmo-gaw-wcc-aerosol-physics.org/wmo-gaw-reports.html>). No clear consensus or published recommendation for the AE33 specific global scattering correction factor C_0 yet exist, although it is clear that the correction by the manufacturer is insufficient as such (Laing et al., 2020). The AE33 at Pallas was programmed to change the filter spot automatically every 24h.

2.3.3 MAAP

145 The Multi Angle Absorption Photometer (MAAP) model 5012 (Thermo Scientific) has been frequently used as an absorption reference for the filter-based absorption instrument techniques (Müller et al., 2011). It internally corrects for the scattering artifact by using a simultaneous back-scattering measurement of the filter tape at multiple angles. In general, the data need very little post-processing. MAAP measures absorption at a wavelength of 637 nm. A wavelength shift from the nominal

value was reported by Müller et al. (2011), and requires a correction with a multiplier 1.05. This correction was applied also
150 here. Pallas MAAP was set to report eBC directly at STP conditions and no further corrections were thus applied. In polluted
environments the MAAP internal data averaging procedure can lead to an artifact that needs to be corrected as suggested by
Hyvärinen et al. (2013).

2.3.4 PSAP

The Particle Soot Absorption Photometer (PSAP; Radiance Research) measures aerosol light attenuation at wavelengths 467,
155 530, and 660 nm (Bond et al., 1999). The PSAP, in contrast to the other filter-based techniques used, requires a manual filter
spot change. This was done when the transmittance reported by the instrument decreased from the initial value of 1.0 to a range
of 0.8–0.7. The flow rate of PSAP was set at 1 LPM.

PSAP records the signal, reference and dark count data at 4s time resolution, which was hourly averaged to calculate the
absorption coefficients. The data were corrected with the measured filter spot size and flow rate as suggested by Bond et al.
160 (1999); Ogren (2010). An average of five spot sizes was determined to be $A = 18.63 \text{ mm}^2$. The volumetric flow rate was
measured at 15 different adjusted flow rate settings at the beginning and at the end of the campaign. The results were converted
to standard flow rate and a linear fit was made to the data, resulting in a flow correction factor of 1.12.

The obtained aerosol absorption coefficient was corrected for the filter-tape loading and scattering artifacts using the correc-
tion scheme by Virkkula (2010)

$$165 \quad \sigma_{\text{PSAP},\lambda} = (k_0 + k_1(h_0 + h_1 * \omega_{0,\lambda}) \ln(\text{Tr}_\lambda)) \sigma_{0,\lambda} - s * \sigma_{\text{SP},\lambda}, \quad (4)$$

where k_0 , k_1 , h_0 , h_1 and s are wavelength dependent constants given by Virkkula (2010). Tr_λ is the transmittance measured
by PSAP at a wavelength λ and $\sigma_{\text{SP},\lambda}$ are the corresponding scattering coefficients. The scattering coefficients were measured
with a nephelometer (TSI Inc. model 3563) and interpolated to the three PSAP wavelengths using the calculated Ångström
exponent values $\alpha_{\text{SP},\lambda}$. The single scattering albedo $\omega_{0,\lambda}$ in Equation 4 was iterated until no significant change in $\sigma_{\text{PSAP},\lambda}$ was
170 observed. At large values of $\omega_{0,\lambda}$ such as here, this correction scheme approaches the widely applied Bond-Ogren correction
scheme (Bond et al., 1999; Ogren, 2010). However, it should be noted that at high $\omega_{0,\lambda}$ values the $\alpha_{\text{AP},\lambda}$ becomes uncertain
and should be interpreted with caution (Backman et al., 2014).

2.3.5 COSMOS

The continuous soot monitoring system (COSMOS) measures light attenuation at a wavelength of 565 nm. The measurement
175 principle is similar to the other filter-based absorption photometers but differs in a sample pre-treatment (Miyazaki et al.,
2008; Kondo et al., 2009). In the COSMOS inlet the volatile non-refractory aerosol components are removed by heating
the sample to 300°C (Kondo et al., 2009). The COSMOS mechanical and optical design with the determined instrument
detection limit and measurement uncertainties are presented by Miyazaki et al. (2008). Due to efficient elimination of the
aerosol scattering related artifacts this method is typically found in good agreement with the thermal-optical and the laser-
180 induced incandescence techniques (Kondo et al., 2009, 2011), and not directly comparable to other filter-based absorption

measurements. Each COSMOS is calibrated against a standard COSMOS instrument using ambient absorbing aerosol within an accuracy of about 5%. The standard COSMOS, in turn, is calibrated by SP2 using ambient absorbing aerosol and applying an aerosol specific MAC. At Pallas, we applied a MAC of $8.73 \text{ m}^2 \text{ g}^{-1}$ to calculate the absorption coefficient from the COSMOS data (Sinha et al., 2017). Detailed comparison of COSMOS and SP2 measurements at several sites in Asia and the Arctic have
185 demonstrated that the overall accuracy in the absorbing aerosol mass concentration measurement is about 10% (Sinha et al., 2017; Ohata et al., 2019, 2020). The stability of MAC is explained by the elimination of the artifacts from aerosol scattering. At Pallas, COSMOS was operated at 0.7 LPM flow rate (STD) and the data was saved every 1-min.

2.3.6 SP2

The single particle soot photometer (SP2, Droplet Measurement Technologies Inc.) measures refractory black carbon (rBC)
190 mass in particles $>70 \text{ nm}$ in diameter (Schwarz et al., 2006). The measurement principle is based on a laser-induced incandescence where the particle is heated up to the point of incandescence which is picked up by the instruments detectors (Stephens et al., 2003). The incandescence signal is proportional to the mass of the refractory black carbon which is calculated particle-by-particle to obtain the rBC mass concentration (Laborde et al., 2012). This technique is both sensitive and accurate and is here used as a reference for the rBC mass concentration in the field.

195 2.3.7 CAPS

The cavity attenuated phase shift light extinction monitor (CAPS PMex, Aerodyne Research Inc.) instrument measures total light extinction by aerosol particles ($\sigma_{EP,\lambda}$) utilizing a cavity attenuated phase shift principle (Kebabian et al., 2007; Massoli et al., 2010; Petzold et al., 2013; Perim de Faria et al., 2017). An updated model of CAPS_{ex} is the CAPS PM_{ssa} (CAPS_{ssa}, Aerodyne Research Inc.). CAPS_{ssa} additionally measures the aerosol light scattering allowing the single scattering albedo
200 to be determined with a single instrument (Onasch et al., 2015; Modini et al., 2021). The scattering measurement technique is similar to an integrating nephelometer, and utilizes a Lambertian integrating sphere in the sample cell. The aerosol light scattering measurement by CAPS_{ssa} is affected by background, truncation and light-source related uncertainties for which calibration is needed.

Aerosol extinction measurement with CAPS is nearly a calibration free technique as long as frequent baseline measurements
205 are performed. A potential source of systematic bias is the geometry correction factor. This is generally a stable constant but has been shown to vary between instruments of even the same model (Petzold et al., 2013; Onasch et al., 2015). An accurate aerosol extinction measurement thus requires calibration against a calibrated scattering instrument, generally a nephelometer.

CAPS_{ex} and CAPS_{ssa} that were operated at Pallas both measure at a wavelength of 630 nm. They were calibrated in the beginning, middle and end of the campaign using ammonium sulfate aerosol generated with an atomizer.

210 2.3.8 Nephelometer

Aerosol light scattering is continuously monitored at Pallas Sammaltunturi site with an integrating nephelometer (TSI3; TSI, model 3563) (Anderson and Ogren, 1998; Heintzenberg et al., 2006). It measures aerosol total scattering and back-scattering fraction at three wavelengths: 450 nm, 550 nm and 700 nm. Nephelometer data were corrected for truncation as suggested by Anderson and Ogren (1998) and converted to standard atmospheric conditions (STP).

215 During the EMPIR campaign the aerosol light scattering was also measured with an Aurora integrating polar nephelometer (AUR4; Ecotech, model 4000) at two angles: 90 and 180. In this setup, the Aurora nephelometer measures the total scattering (180) and back-scattering (90) of the aerosol in similar manner as the TSI nephelometer. The Aurora 4000 measures scattering at wavelengths of 450 nm, 525 nm, and 635 nm. Data were corrected for truncation based on Müller et al. (2011) and converted to STP.

220 A zero check was performed daily for both nephelometers and they were calibrated with CO₂ gas in the beginning and in the end of the campaign.

2.3.9 Extinction Minus Scattering (EMS)

An indirect technique to determine the aerosol light absorption is based on separately measured aerosol extinction and aerosol scattering (Strawa et al., 2003; Virkkula et al., 2005; Modini et al., 2021). This extinction minus scattering (EMS) -method
225 relies on those aerosol optical properties that can be accurately determined using existing techniques. It is also traceable to SI units. The EMS method avoids the artifacts encountered with filter-based techniques.

In Pallas the aerosol light scattering was measured with two integrating nephelometers and the extinction with CAPSex and CAPSssa instruments. Two instrument "pairs" were formed: (1) Aurora 4000 polar nephelometer and CAPSssa (both were part of campaign instrumentation) and (2) CAPSex and the TSI nephelometer (permanent instrumentation at site). These methods
230 here are referred to as EMS₁ and EMS₂, respectively. The CAPSssa scattering and extinction measurement alone was also used to determine aerosol absorption, which is here referred to as method EMS₃.

In the beginning, middle and end of the campaign the CAPS instruments data were calibrated against the nephelometers. Purely scattering ammonium sulphate aerosol was produced with an atomizer (TOPAS, model ATM230). The aerosol losses in the sampling lines and in the instruments are size dependent and the $\alpha_{SP,\lambda}$ reflects the optical size of the aerosol. In Pallas
235 summer atmosphere a typical value of $\alpha_{SP,\lambda} = 1.5 - 1.7$ (Lihavainen et al., 2015). The ammonium sulphate calibrations were performed at this $\alpha_{SP,\lambda}$ range so that the calibrations will be valid for the ambient aerosol as well. A summary of the three calibrations proposed multipliers of 1.21 (EMS₁) and 1.04 (EMS₂) for CAPS data (Figure S1). These correction factors were applied to all CAPS data in this manuscript. The different correction factors for the CAPSex and CAPSssa could be explained by the different individual geometry correction factors. The two CAPS were having identical flow rates and inlet settings, and
240 the two nephelometers (reference points) had a small difference in flow rates and in inlet tubing sizes which could to a minor part also explain the differences in correction factors. Major care was taken in measurement system construction to provide similar sample intake to all instruments.

2.4 Sampling

The bulk of the instruments were connected to a common inlet which was equipped with a Particulate Matter (PM) 10 μm cut-size aerosol inlet head and a nafion permature model MD-700-48 aerosol drier. The relative humidity (RH) of the sample in the entrance of the inlet was monitored to remain $<40\%$ throughout the campaign. The total flow of 18.3 LPM was divided for the instruments via a self-made flow-divider that consisted of six cylinder symmetric exit tubes. One of the exits was further divided using a TSI laminar flow-divider into two flows, one for each extinction monitor (CAPSex and CAPSssa, see Table 1). In addition, two instruments (SP2 and AE31, see Table 1) were connected to a slightly heated, total aerosol inlet about 3 m apart from the PM10 line. The AE31 is measuring in this inlet year-round and the SP2 has a limited measurement size range for which the inlet cut-size does not affect the result in cloud-free conditions.

3 Results

3.1 Allan variance analysis on absorption methods stability and detection limits

Detection limits and optimal averaging times for the absorption measurement instruments were defined using Allan variance analysis. Allan variances describe the time-averaged stability of a series of consecutive measurements and can be used to estimate noise processes (Allan, 1966; Werle et al., 1993). They determine the data variability by analyzing the sum of the squared differences between the measurements subsets in such a way that if N is the number of subsets of y_j measurements, the Allan variance for period t is defined as

$$\sigma_y^2(t) = \frac{1}{2(N-1)} \sum_{j=1}^{N-1} (y_{j+1} - y_j)^2. \quad (5)$$

The Allan variances can be used to find the optimal averaging time that minimizes the noise without sacrificing the signal. For a white noise dominated system the square root of the variance, called Allan deviation, is equal to the standard deviation of the mean giving directly the 1σ detection limit (Werle et al., 1993).

Noise in the measured absorption signal was determined during a 6hs period of clean, particle-free measurements. Allan deviation for the different absorption methods in this study was calculated for data averaging times from 1-min to 6hs (Figure 1). PSAP showed the lowest Allan deviation minimum followed by AE33, COSMOS, MAAP and AE31 (Figure 1a). The EMS methods showed about an order of magnitude higher Allan deviation compared to the filter-based methods (Figure 1b). The minimum Allan deviation in PSAP data was observed at around 1h averaging time after which a strong increase ($1/t$ - dependence) in noise occurred. Deviation from the typical behavior of a white noise dominated system (i.e. $1/\sqrt{t}$ -dependence) can be expected for PSAP as was shown by Springston et al. (2007). The increasing Allan deviation of PSAP data at averaging times $>1\text{h}$ indicates system drifts and a similar effect could be interpreted to take place in AE33 and COSMOS data at around 2.5hs. The EMS methods show a constant decrease of a white noise signal at higher than 10-min averaging times. Out of the three EMS methods used, the EMS3 that measured both extinction and scattering with one instrument, here presented the

lowest noise. While it is known that the EMS method is very sensitive to error amplification, the accuracy of this result can still be compromised (Modini et al., 2021).

275 The 1σ detection limits of different methods to measure $\sigma_{AP,637nm}$ were calculated as an average of the Allan deviation between 1–2 hs averaging times and are presented in Table 2. The stability analysis also justifies the use of hourly-averaged data in the further analysis of this work. The lowest detection limit of 0.002 Mm^{-1} was calculated for PSAP, while it was 0.01 Mm^{-1} for MAAP, 0.1 Mm^{-1} for EMS3 and 0.8 Mm^{-1} for EMS2. Qualitatively and in comparison to each others, the instruments detection limits followed those provided by the manufacturers, although the determined 1σ absolute values were
280 all lower (Table 1).

3.2 Aerosol absorption coefficient values measured in Arctic air masses

The absorption instruments were used in parallel to measure atmospheric aerosol in Pallas campaign. Arctic air masses prevailed during all the campaign and correspondingly very low aerosol concentrations were measured (Figure 2). The aerosol was highly scattering, with an average single-scattering albedo of 0.97. These conditions challenged the detection capabilities
285 of the absorption measurement methods used. The aerosol absorption coefficient $\sigma_{AP,630nm}$ measured with filter-based instruments varied between 0 and 0.3 Mm^{-1} (Figure 2). The variability of $\sigma_{AP,630nm}$ with time measured by the EMS methods agreed qualitatively but differed 10-fold in absolute numbers. Based on EMS methods, the $\sigma_{AP,630nm}$ at Pallas varied between 0 and 3 Mm^{-1} .

The median aerosol absorption coefficients $\sigma_{AP,635nm}$ measured by the five filter-based methods during the campaign were
290 within the limits from 0.07 to 0.09 Mm^{-1} (Table 3). The overall median using data from all instruments was 0.08 Mm^{-1} and the 25th and the 75th percentiles were 0.06 and 0.10 Mm^{-1} (Figure 3). The measured atmospheric absorption coefficient values with their standard deviation range exceeded the instruments detection limits for all the five filter-based methods (Table 2). The lowest average $\sigma_{AP,\lambda}$ was measured with COSMOS instrument presenting also the lowest standard deviation (Figure 3). This is expected since the sample pre-treatment in the COSMOS heated inlet effectively removes the particle light scattering
295 coating thereby eliminating the related artifacts. Heating also decreases fluctuations caused by possible sample RH variations. However, the sample modification also changes the aerosol interaction with light which then no longer corresponds to its dry atmospheric state. Therefore, this method is primarily used to determine the mass of the absorbing refractory particles, rather than the aerosol light absorption in the atmosphere. A low standard deviation around the average was also measured by the AE33. The highest average $\sigma_{AP,\lambda}$ was measured by the AE31 instrument. This could be explained by this methods' sensitivity
300 to various artifacts and thus, a significant dependence on the aerosol characteristics.

The EMS methods systematically overestimated the aerosol absorption coefficient, giving a campaign-average medium of 0.59 Mm^{-1} and the 25th and the 75th percentiles of 0.44 and 0.74 Mm^{-1} when considering all EMS data (Figure 3). The absorption values measured at Pallas are clearly below the detection capabilities of the EMS methods, as suggested by the results from the previous section. The baseline drift and error amplification are known to affect the EMS methods detection
305 limits (Modini et al., 2021). The calculated standard deviation around the average $\sigma_{AP,\lambda}$ was more significant than the signal height in all three EMS methods (Table 3).

The measured absorption coefficient values are in the lower end of that typically observed at Pallas site. Lihavainen et al. (2015) long-term analysis showed that the $\sigma_{AP,\lambda}$ in Pallas during summer ranges between 0.1–1 Mm^{-1} , where the lowest values typically correspond to the clean Arctic air flows. Thus, the measured $\sigma_{AP,\lambda}$ values during the campaign are well
310 representative of the values measured around the Arctic during summer (Schmeisser et al., 2018).

3.3 Accuracy of the measured absorption

The accuracy of the filter-based methods was further investigated by comparing them between each others using MAAP as a main campaign-time reference. This choice is justified by the low demand of any artifact related post-correction in MAAP.

Linear correlation between the absorption coefficients measured with different techniques was calculated using the Williamson-
315 York bivariate fitting method provided by Cantrell (2008). This method is less sensitive to outliers than the standard least-squares method, and considers that uncertainties can exist in both fitting variables which here is the case. The correlation statistics (R^2 , slope and intercept with their corresponding standard errors) for the filter-based techniques are presented in Table 4. All correlations were statistically highly significant.

The best correlation was obtained with $\sigma_{AE33,\lambda}$ and $\sigma_{MAAP,\lambda}$, followed by $\sigma_{COSMOS,\lambda}$ and $\sigma_{MAAP,\lambda}$ ($R^2 = 0.87$ and 0.85 ,
320 respectively). Correlation between $\sigma_{AE31,\lambda}$ and $\sigma_{MAAP,\lambda}$ was noisy and resulted in the lowest $R^2 = 0.65$. Both AE31 and PSAP compared to MAAP showed nearly a linear correlation of $\sigma_{AP,\lambda}$, with a slope of 0.95 and 0.93, respectively, and an offset of 0.01. The AE33 appeared to overestimate the $\sigma_{AP,\lambda}$ at the lowest measured absorption values, while it slightly underestimated at the other end of the scale. This led to a correlation slope significantly below one, as compared to MAAP. Both COSMOS and AE33 correlations were low, 0.68 and 0.62, respectively, but in COSMOS this is explained by the sample pre-treatment in inlet
325 which modifies the sample composition. The low correlation slope of AE33 seems to be rather explained by the deviation of data near the zero values. Overestimation of $\sigma_{AP,\lambda}$ at values close to zero as compared to MAAP was notable in all instruments data, except in AE31 (Figure 4).

Figure 4 additionally shows that aerosol absorption increases with decreasing single scattering albedo ω_0 . This can be a real effect but can also partly relate with the decreasing accuracy in $\sigma_{AP,\lambda}$ result at the edge of the instruments detection limits,
330 affecting the scattering to absorption ratio.

Given that the measured absorption coefficients are close to the detection limits of the instruments the obtained correlations are reasonably good. Slopes and intercepts could be modified with a different selection of data outliers which at such low concentrations can be a sensitive choice. Comparison of $\sigma_{AP,\lambda}$ measured with EMS methods to the hourly-averaged values from MAAP did not lead to statistically highly significant correlations.

335 3.4 Mass absorption cross-section of Arctic aerosol

To estimate the absorbing particle mass based on the measured absorption coefficient, a suitable value of mass absorption cross-section (MAC) is needed. We defined the average MAC during our campaign by comparing the measured absorption by MAAP with the measured rBC mass by SP2. This resulted in a MAC value of $16.0 \text{ m}^2 \text{ g}^{-1}$ (Figure 5). The default MAC in

MAAP is $6.6 \text{ m}^2 \text{ g}^{-1}$, which gives a ratio of 2.4 between the black carbon mass equivalent and the refractory black carbon
340 mass.

The MAC is not a constant value and can depend on various factors such as the absorbing aerosol source and the aerosol
mixing state that is subject to its atmospheric aging (Jacobson, 2001; Slowik et al., 2007; Petzold et al., 2013; Ohata et al.,
2020). Recently, a comprehensive characterization of the Arctic MAC values was published by Ohata et al. (2020). Their results
were calculated for a dataset covering a broad range of absorption values measured around the Arctic using COSMOS as a
345 reference mass monitor. The overall average MAC in their study was $14.0 \text{ m}^2 \text{ g}^{-1}$, and thus on the same order of magnitude
as obtained here for Pallas site when comparing MAAP directly with the SP2.

4 Conclusions

Absorbing aerosol characteristics were measured by various methods and instruments in an EMPIR BC month long measure-
ment campaign at remote Pallas station in northern Finland. Arctic air masses prevailed and consequently very clean and highly
350 scattering aerosol persisted throughout the campaign. This was a challenge for the absorption instrumentation in terms of their
accuracy and detection limits.

We determined the 1σ -detection limits of $\sigma_{AP,637nm}$ for five filter-based absorption monitors: MAAP, AE31, AE33, PSAP,
COSMOS, and for the extinction minus scattering (EMS) method with three different instrument pairs using Allan variance
analysis. The detection limits of filter-based instruments were in range $0.002 \text{ Mm}^{-1} - 0.014 \text{ Mm}^{-1}$. The lowest detection
355 limit was calculated for PSAP and the highest for AE31. The detection limits of EMS methods were an order of magnitude
higher, ranging from 0.38 to 0.11 Mm^{-1} . As a general rule our results suggest that the filter-based absorption instruments can
be applied down to $\sigma_{AP,\lambda} = 0.01 \text{ Mm}^{-1}$ values and the EMS methods up from $\sigma_{AP,\lambda} > 0.1 \text{ Mm}^{-1}$.

The aerosol absorption coefficient measured at Pallas ranged from 0.06 to 0.10 Mm^{-1} (representing the 25th to 75th per-
centiles) and the different filter-based instruments agreed approximately within 15–20%. AE33 showed the best linear corre-
360 lation with MAAP ($R^2 = 0.87$), followed by COSMOS ($R^2 = 0.85$) and PSAP ($R^2 = 0.78$). The noisy data of AE31 resulted
in a slightly lower, yet a highly significant, correlation ($R^2 = 0.65$). A positive bias at low $\sigma_{AP,\lambda}$ values near zero levels was
observed in AE33, PSAP and COSMOS. The correlation slope with MAAP was close to one in PSAP and AE31, but clearly
below one in COSMOS and AE33. It has to be kept in mind that these results were calculated for a very clean environment
and at a relatively narrow $\sigma_{AP,\lambda}$ range from 0 to 0.3 Mm^{-1} . Thus the biases observed at around zero concentrations can affect
365 significantly the correlation slopes.

Finally, we determined the aerosol MAC value during the campaign using SP2 as a mass reference and MAAP as an
absorption reference. The MAC, determined as a slope of the correlation between those two, was $16.0 \text{ m}^2 \text{ g}^{-1}$ and is thus in
good agreement with previous similar Arctic MAC studies.

Overall, the filter-based absorption instruments are shown to be a robust and sensitive method to measure absorption in
370 pristine environments, such as the Arctic. Future studies should focus on providing the means for field instruments reference
and calibration methods to further improve the accuracy of the filter-based methods.

Data availability. Pallas WMO Global Atmospheric Watch (GAW) station, part of the Aerosols, Clouds, and Trace gases Research InfraS-
tructure (ACTRIS), submits aerosol number, size, scattering and absorption measurement data annually to EBAS database operated at the
Norwegian Institute for Air Research (NILU) (<http://ebas.nilu.no>). These data are available at no cost and can be used in agreement with
375 the ACTRIS Data Policy statement. The specific data measured during EMPIR BC campaign are available for scientific use upon request.
Aurora 4000 data are available at TROPOS, CAPS data at DEMOKRITOS and all other data at FMI by contacting the corresponding data
owner and co-author in this manuscript.

Author contributions. EA, HS, JB, MG, KE, TM and AH participated in planning the campaign. EA, JB, HS and MG made the measure-
ments. EA analysed the filter-based instrument absorption data and all auxiliary data with contributions from AV and JB. JB analysed SP2
380 data. MG and KE analysed CAPS data. TM analysed Aurora nephelometer data. SO, YK and HS analysed COSMOS data. EA prepared the
paper with contributions from all authors.

Competing interests. Authors do not declare any competing interests.

Acknowledgements. We greatly acknowledge the funding from the 16ENV02 Black Carbon project of the European Union through the
European Metrology Programme for Innovation and Research (EMPIR). The financial support of the ACTRIS by the European Union's
385 Horizon 2020 research and innovation programme under grant agreement no. 654109 is also gratefully acknowledged. This research was
also supported by Academy of Finland via project NABCEA (grant no. 29664) and by Business Finland via project BC Footprint (grant no.
49402-201040). This work was also supported by the Environmental Research and Technology Development Fund (2-2003), and the Arctic
Challenge for Sustainability II (ArCS II) project of Japan.

References

- 390 Allan, D. W.: Statistics of Atomic Frequency Standards, *Proc. IEEE*, 54, 221–230, 1966.
- Anderson, T. L., and Ogren, J. A.: Determining aerosol radiative properties using the TSI 3563 integrating nephelometer, *Aerosol Sci. Tech.*, 29, 57–69, <https://doi.org/10.1080/02786829808965551>, 1998.
- Arnott, W. P., Moosmüller, H., Rogers, C. F., Jin, T., and Bruch, R.: Photoacoustic spectrometer for measuring light absorption by aerosol: Instrument description, *Atmos. Environ.*, 33, 2845–2852, [https://doi.org/10.1016/S1352-2310\(98\)00361-6](https://doi.org/10.1016/S1352-2310(98)00361-6), 1999.
- 395 Arnott, W. P., Hamasha, K., Moosmüller, H., Sheridan, P. J., and Ogren, J. A.: Towards aerosol light-absorption measurements with a 7-wavelength aethalometer: evaluation with a photoacoustic instrument and 3-wavelength nephelometer, *Aerosol Sci. Tech.*, 39(1), 17–29, <https://doi.org/10.1080/027868290901972>, 2005.
- Backman, J., Virkkula, A., Vakkari, V., Beukes, J. P., Van Zyl, P. G., Josipovic, M., Piketh, S., Tiitta, P., Chiloane, K., Petäjä, T., Kulmala, M., and Laakso, L.: Differences in aerosol absorption Ångström exponents between correction algorithms for a particle soot absorption photometer measured on the South African Highveld, *Atmos. Meas. Tech.*, 7, 4285–4298, <https://doi.org/10.5194/amt-7-4285-2014>, 2014.
- 400 Backman, J., Schmeisser, L., Virkkula, A., Ogren, J. A., Asmi, E., Starkweather, S., Sharma, S., Eleftheriadis, K., Uttal, T., Jefferson, A., Bergin, M., Makshtas, A., Tunved, P., and Fiebig, M.: On Aethalometer measurement uncertainties and an instrument correction factor for the Arctic, *Atmos. Meas. Tech.*, 10, 5039–5062, <https://doi.org/10.5194/amt-10-5039-2017>, 2017.
- Bond, T. C., Anderson, T. L., and Campbell, D.: calibration and intercomparison of filter-based measurements of visible light absorption by aerosols, *Aerosol Sci. Tech.*, 30(6), 582–600, <https://doi.org/10.1080/027868299304435>, 1999.
- 405 Bond, T. C., and Bergstrom, R. W.: Light Absorption by Carbonaceous Particles: An Investigative Review, *Aerosol Sci. Technol.*, 40, 27–67, 2006.
- Cantrell, C. A.: Technical Note: Review of methods for linear least-squares fitting of data and application to atmospheric chemistry problems, *Atmos. Chem. Phys.*, 8, 5477–5487, <https://doi.org/10.5194/acp-8-5477-2008>, 2008.
- 410 Collaud Coen, M., Weingartner, E., Apituley, A., Ceburnis, D., Fierz-Schmidhauser, R., Flentje, H., Henzing, J. S., Jennings, S. G., Moerman, M., Petzold, A., Schmid, O., and Baltensperger, U.: Minimizing light absorption measurement artifacts of the Aethalometer: evaluation of five correction algorithms, *Atmos. Meas. Tech.*, 3, 457–474, <https://doi.org/10.5194/amt-3-457-2010>, 2010.
- Drinovec, L., Močnik, G., Zotter, P., Prévôt, A. S. H., Ruckstuhl, C., Coz, E., Rupakheti, M., Sciare, J., Müller, T., Wiedensohler, A., and Hansen, A. D. A.: The "dual-spot" Aethalometer: an improved measurement of aerosol black carbon with real-time loading compensation, *Atmos. Meas. Tech.*, 8, 1965–1979, <https://doi.org/10.5194/amt-8-1965-2015>, 2015.
- 415 Hagler, G., Vedantham, R., and Turner, J.: Post-processing Method to Reduce Noise while Preserving High Time Resolution in Aethalometer Real-time Black Carbon Data. *Aerosol Air Qual. Res.*, 11, 539–546, 2011.
- Hansen, A. D. A., Rosen, H., and Novakov, T.: Real-time measurement of the absorption coefficient of aerosol particles, *Appl. Opt.*, 21, 3060–3062, <https://doi.org/10.1364/AO.21.003060>, 1982.
- 420 Hansen, A. D. A., Rosen, H., and Novakov, T.: The aethalometer – An instrument for the real-time measurement of optical absorption by aerosol particles, *Sci. Total Environ.*, 36, 191, [https://doi.org/10.1016/0048-9697\(84\)90265-1](https://doi.org/10.1016/0048-9697(84)90265-1), 1984.
- Hatakka J., Aalto T., Aaltonen V., Aurela M., Hakola H., Komppula M., Laurila T., Lihavainen H., Paatero J., Salminen K., and Viisanen Y.: Overview of the atmospheric research activities and results at Pallas GAW station, *Boreal Env. Res.*, 8, 365–383, 2003.

- Heintzenberg, J., Wiedensohler, A., Tuch, T. M., Covert, D. S., Sheridan, P., Ogren, J. A., Gras, J., Nessler, R., Kleefeld, C., Kalivitis, N.,
425 Aaltonen, V., Wilhelm, R. T., and Havlicek, M.: Intercomparisons and aerosol calibrations of 12 commercial integrating nephelometers of
three manufacturers, *J. Atmos. Oceanic. Technol.*, 23(7), 902–914, <https://doi.org/10.1175/JTECH1892.1>, 2006.
- Hyvärinen, A.-P., Vakkari, V., Laakso, L., Hooda, R. K., Sharma, V. P., Panwar, T. S., Beukes, J. P., van Zyl, P. G., Josipovic, M., Garland,
R. M., Andreae, M. O., Pöschl, U., and Petzold, A.: Correction for a measurement artifact of the Multi-Angle Absorption Photometer
(MAAP) at high black carbon mass concentration levels, *Atmos. Meas. Tech.*, 6, 81–90, <https://doi.org/10.5194/amt-6-81-2013>, 2013.
- 430 Jacobson, M. Z.: Strong radiative heating due to the mixing state of Black Carbon in atmospheric aerosols, *Nature*, 409, 695–697, 2001.
- Kanaya, Y., Komazaki, Y., Pochanart, P., Liu, Y., Akimoto, H., Gao, J., Wang, T., and Wang, Z.: Mass concentrations of black
carbon measured by four instruments in the middle of Central East China in June 2006, *Atmos. Chem. Phys.*, 8, 7637–7649,
<https://doi.org/10.5194/acp-8-7637-2008>, 2008.
- Kebabian, P. L., Robinson, W. A., and Freedman, A.: Optical extinction monitor using cw cavity enhanced detection, *Rev. Sci. Instrum.*,
435 78(6), 063102, <https://doi.org/10.1063/1.2744223>, 2007.
- Kondo, Y., Sahu, L., Kuwata, M., Miyazaki, Y., Takegawa, N., Moteki, N., Imaru, J., Han, S., Nakayama, T., Kim Oanh, N. T., Hu, M., Kim,
Y. J., and Kita, K.: Stabilization of the mass absorption cross section of black carbon for filter-based absorption photometry by the use of
a heated inlet, *Aerosol Sci. Tech.*, 43(8), 741–756, <https://doi.org/10.1080/02786820902889879>, 2009.
- Kondo, Y., Sahu, L., Moteki, N., Khan, F., Takegawa, N., Liu, X., Koike, M., and Miyakawa, T.: Consistency and traceability of black
440 carbon measurements made by laser-induced incandescence, thermal-optical transmittance, and filter-based photo-absorption techniques,
Aerosol Sci. Tech., 45(2), 295–312, <https://doi.org/10.1080/02786826.2010.533215>, 2011.
- Laborde, M., Schnaiter, M., Linke, C., Saathoff, H., Naumann, K.-H., Möhler, O., Berlenz, S., Wagner, U., Taylor, J. W., Liu, D., Flynn, M.,
Allan, J. D., Coe, H., Heimerl, K., Dahlkötter, F., Weinzierl, B., Wollny, A. G., Zannata, M., Cozic, J., Laj, P., Hitznerberger, R., Schwarz,
J. P. and Gysel, M.: Single Particle Soot Photometer intercomparison at the AIDA chamber, *Atmos. Meas. Tech.*, 5(12), 3077–3097,
445 [doi:10.5194/amt-5-3077-2012](https://doi.org/10.5194/amt-5-3077-2012), 2012.
- Laing, J.R., Jaffe, D.A., and Sedlacek, III, A.J.: Comparison of filter-based absorption measurements of biomass burning aerosol and back-
ground aerosol at the Mt. Bachelor Observatory. *Aerosol Air Quality Research* 20, 663–678, 2020. doi: 10.4209/aaqr.2019.06.0298.
- Lihavainen, H., Hyvärinen, A., Asmi, E., Hatakka, J., and Viisanen, Y.: Long-term variability of aerosol optical properties in northern Finland,
Boreal Env. Res., 20, 526–541, <http://hdl.handle.net/10138/228289>, 2015.
- 450 Lohila A., Penttilä T., Jortikka S., Aalto T., Anttila P., Asmi E., Aurela M., Hatakka J., Hellén H., Henttonen H., Hänninen P., Kilkki J.,
Kyllönen K., Laurila T., Lepistö A., Lihavainen H., Makkonen U., Paatero J., Rask M., Sutinen R., Tuovinen J.-P., Vuorenmaa J., and
Viisanen Y.: Preface to the special issue on integrated research of atmosphere, ecosystems and environment at Pallas, *Boreal Env. Res.*,
20, 431–454, <http://hdl.handle.net/10138/228278>, 2015.
- Massoli, P., Kebabian, P. L., Onasch, T. B., Hills, F. B., and Freedman, A.: Aerosol Light Extinction Measurements by Cavity Attenuated
455 Phase Shift (CAPS) Spectroscopy: Laboratory validation and field deployment of a compact aerosol particle extinction monitor, *Aerosol
Sci. Tech.*, 44, 428–435, <https://doi.org/10.1080/02786821003716599>, 2010.
- Miyazaki, Y., Kondo, Y., Sahu, L. K., Imaru, J., Fukushima, N., and Kanno, A.: Performance of a newly designed continuous soot monitoring
system (COSMOS), *J. Environ. Monitor.*, 10, 1195–1201, <https://doi.org/10.1039/B806957C>, 2008.
- Modini, R. L., Corbin, J. C., Brem, B. T., Irwin, M., Bertò, M., Pileci, R. E., Fetfatzis, P., Eleftheriadis, K., Henzing, B., Moerman, M.
460 M., Liu, F., Müller, T., and Gysel-Beer, M.: Detailed characterization of the CAPS single-scattering albedo monitor (CAPS PM_{ssa}) as a

- field-deployable instrument for measuring aerosol light absorption with the extinction-minus-scattering method, *Atmos. Meas. Tech.*, 14, 819–851, <https://doi.org/10.5194/amt-14-819-2021>, 2021.
- Moosmuller, H., Chakrabarty, R.K., and Arnott, W.: Aerosol light absorption and its measurement: A review, *J. Quant. Spectrosc. Radiat. Transf.*, 110, 844–878, <https://doi.org/10.1016/j.jqsrt.2009.02.035>, 2009.
- 465 Müller, T., Henzing, J. S., de Leeuw, G., Wiedensohler, A., Alastuey, A., Angelov, H., Bizjak, M., Collaud Coen, M., Engström, J. E., Gruening, C., Hillamo, R., Hoffer, A., Imre, K., Ivanow, P., Jennings, G., Sun, J. Y., Kalivitis, N., Karlsson, H., Komppula, M., Laj, P., Li, S.-M., Lunder, C., Marinoni, A., Martins dos Santos, S., Moerman, M., Nowak, A., Ogren, J. A., Petzold, A., Pichon, J. M., Rodriguez, S., Sharma, S., Sheridan, P. J., Teinilä, K., Tuch, T., Viana, M., Virkkula, A., Weingartner, E., Wilhelm, R., and Wang, Y. Q.: Characterization and intercomparison of aerosol absorption photometers: result of two intercomparison workshops, *Atmos. Meas. Tech.*, 4, 245–268, <https://doi.org/10.5194/amt-4-245-2011>, 2011a.
- 470 Müller, T., Laborde, M., Kassel, G., and Wiedensohler, A.: Design and performance of a three-wavelength LED-based total scatter and backscatter integrating nephelometer, *Atmos. Meas. Tech.*, 4, 1291–1303, <https://doi.org/10.5194/amt-4-1291-2011>, 2011b.
- Nakayama, T., Kondo, Y., Moteki, N., Sahu, L. K., Kinase, T., Kita, K., and Matsumi, Y.: Size-dependent correction factors for absorption measurements using filter-based photometers: PSAP and COSMOS, *J. Aerosol Sci.*, 41, 333–343, <https://doi.org/10.1016/j.jaerosci.2010.01.004>, 2010.
- 475 Ogren, J. A.: Comment on ‘Calibration and intercomparison of filter-based measurements of visible light absorption by aerosols’, *Aerosol Sci. Tech.*, 44(8), 589–591, <https://doi.org/10.1080/02786826.2010.482111>, 2010.
- Ohata, S., Kondo, Y., Moteki, N., Mori, T., Yoshida, A., Sinha, P. R., and Koike, M.: Accuracy of black carbon measurements by a filter-based absorption photometer with a heated inlet, *Aerosol Sci. Tech.* 53(9), 1079–91, <https://doi.org/10.1080/02786826.2019.1627283>, 2019.
- 480 Ohata, S., Mori, T., Kondo, Y., Sharma, S., Hyvärinen, A., Andrews, E., Tunved, P., Asmi, E., Backman, J., Servomaa, H., Veber, D., Koike, M., Kanaya, Y., Yoshida, A., Moteki, N., Zhao, Y., Matsushita, J., and Oshima, N.: Estimates of mass absorption cross sections of black carbon for filter-based absorption photometers in the Arctic, *Atmos. Chem. Phys. Discuss.* [preprint], <https://doi.org/10.5194/acp-2020-1190>, 2020.
- Onasch, T. B., Massoli, P., Keabian, P. L., Hills, F. B., Bacon, F. W., and Freedman, A.: Single Scattering Albedo Monitor for Airborne Particulates, *Aerosol Sci. Tech.*, 49, 267–279, <https://doi.org/10.1080/02786826.2015.1022248>, 2015.
- 485 Perim de Faria, J., Bundke, U., Berg, M., Freedman, A., Onasch, T. B., and Petzold, A.: Airborne and laboratory studies of an IAGOS instrumentation package containing a modified CAPS particle extinction monitor, *Aerosol Sci. Tech.*, 1–14, <https://doi.org/10.1080/02786826.2017.1355547>, 2017.
- Petzold, A., Ogren, J. A., Fiebig, M., Laj, P., Li, S.-M., Baltensperger, U., Holzer-Popp, T., Kinne, S., Pappalardo, G., Sugimoto, N., Wehrli, C., Wiedensohler, A., and Zhang, X.-Y.: Recommendations for reporting "black carbon" measurements, *Atmos. Chem. Phys.*, 13, 8365–8379, <https://doi.org/10.5194/acp-13-8365-2013>, 2013a.
- 490 Petzold, A., Onasch, T., Keabian, P., and Freedman, A.: Intercomparison of a Cavity Attenuated Phase Shift-based extinction monitor (CAPS PMex) with an integrating nephelometer and a filter-based absorption monitor, *Atmos. Meas. Tech.*, 6, 1141–1151, <https://doi.org/10.5194/amt-6-1141-2013>, 2013b.
- 495 Reid, J. S., Hobbs, P. V., Liousse, C., Martins, J. V., Weiss, R. E. and Eck, T. F.: Comparisons of techniques for measuring short-wave absorption and black carbon content of aerosols from biomass burning in Brazil. *J. Geophys. Res.-Atmos.* 103, 32031–32040, <https://doi.org/10.1029/98JD00773>, 1998.

- Rosen, H., Hansen, A. D. A., Gundel, L., and Novakov, T.: Identification of the optically absorbing component in urban aerosols, *Appl. Opt.*, 17, 3859–3861, <https://doi.org/10.1364/AO.17.003859>, 1978.
- 500 Saathoff, H., Naumann, K. H., Schnaiter, M., Schock, W., Weingartner, E., Baltensperger, U., Kramer, L., Bozoki, Z., Pöschl, U., Niessner, R., and Schurath, U.: Carbon mass determinations during the AIDA soot aerosol campaign 1999, *J. Aerosol Sci.*, 34(10), 1399–1420, [https://doi.org/10.1016/S0021-8502\(03\)00365-3](https://doi.org/10.1016/S0021-8502(03)00365-3), 2003.
- Schmeisser, L., Backman, J., Ogren, J. A., Andrews, E., Asmi, E., Starkweather, S., Uttal, T., Fiebig, M., Sharma, S., Eleftheriadis, K., Vratolis, S., Bergin, M., Tunved, P., and Jefferson, A.: Seasonality of aerosol optical properties in the Arctic, *Atmos. Chem. Phys.*, 18, 11599–11622, <https://doi.org/10.5194/acp-18-11599-2018>, 2018.
- 505 Schmid, O., Artaxo, P., Arnott, W. P., Chand, D., Gatti, L. V., Frank, G. P., Hoffer, A., Schnaiter, M., and Andreae, M. O.: Spectral light absorption by ambient aerosols influenced by biomass burning in the Amazon Basin. I: Comparison and field calibration of absorption measurement techniques, *Atmos. Chem. Phys.*, 6, 3443–3462, <https://doi.org/10.5194/acp-6-3443-2006>, 2006.
- Schulz, C., Kock, B., Hofmann, M., Michelsen, H.A., Will, S., Bougie, B., Suntz, R., and Smallwood, G.: Laser-induced incandescence: 510 Recent trends and current questions, *J. Appl. Phys. B.*, 83, 333–354, <https://doi.org/10.1007/s00340-006-2260-8>, 2006.
- Schwarz, J. P., Gao, R. S., Fahey, D. W., Thomson, D. S., Watts, L. A., Wilson, J. C., Reeves, J. M., Darbeheshti, M., Baumgardner, D. G., Kok, G. L., Chung, S. H., Schulz, M., Hendricks, J., Lauer, A., Kaercher, B., Slowik, J. G., Rosenlof, K. H., Thompson, T. L., Langford, A. O., Loewenstein, M. and Aikin, K. C.: Single-particle measurements of midlatitude black carbon and light scattering aerosols from the boundary layer to the lower stratosphere, *J. Geophys. Res.-Atmos.*, 111, D16, <https://doi.org/10.1029/2006JD007076>, 2006.
- 515 Sinha, P. R., Kondo, Y., Koike, M., Ogren, J. A., Jefferson, A., Barrett, T. E., Sheesley, R. J., Ohata, S., Moteki, N., Coe, H., Liu, D., Irwin, M., Tunved, P., Quinn, P. K., and Zhao, Y.: Evaluation of ground-based black carbon measurements by filter-based photometers at two Arctic sites, *J. Geophys. Res. Atm.*, 122(6), 3544–3572, 2017. <https://doi.org/10.1002/2016JD025843>
- Slowik, J. G., Cross, E. S., Han, J-H, Davidovits, P., Onasch, T. B., Jayne, J. T., Williams, L. R., Canagaratna, M. R., Worsnop, D. R., Chakrabarty, R. K., Moosmüller, H., Arnott, W. P., Schwarz, J. P., Gao, R-S., Fahey, D. W., David W. Kok, G. L., and Pet- 520 zold, A.: An inter-comparison of instruments measuring black carbon content of soot particles, *Aerosol Sci. Tech.*, 41(3), 295–314, <https://doi.org/10.1080/02786820701197078>, 2007.
- Springston, S. R., and Sedlacek III, A. J.: Noise Characteristics of an Instrumental Particle Absorbance Technique, *Aerosol Sci. Tech.*, 41(12), 1110–1116, 2007. DOI: 10.1080/02786820701777457
- Stephens, M., Turner, N., and Sandberg, J.: Particle identification by laser-induced incandescence in a solid-state laser cavity, *Appl. Opt.*, 42, 525 3726–3736, <https://doi.org/10.1364/AO.42.003726>, 2003.
- Strawa, A., Castaneda, R., Owano, T., Baer, D., Paldus, B., and Gore, W.: The measurement of aerosol optical properties using continuous wave cavity ring-down techniques, *J. Atmos. Oceanic Technol.*, 20(4), 454–465, [https://doi.org/10.1175/1520-0426\(2003\)20<454:TMOAOP>2.0.CO;2](https://doi.org/10.1175/1520-0426(2003)20<454:TMOAOP>2.0.CO;2), 2003.
- Tørseth, K., Andrews, E., Asmi, E., Eleftheriadis, K., Fiebig, M., Herber, A., Lin, H., Kylling, A., Lupi, A., Massling, A., Mazzola, M., 530 Nøjgaard, J.K., Popovicheva, O., Schichtel, B., Schmale, J., Sharma, S., Skov, H., Stebel, K., Vassel, B., Vitale, V., Whaley, C., Yttri, K.E., and Zanatta, M.: Review of Observation Capacities and Data Availability for Black Carbon in the Arctic Region: EU Action on Black Carbon in the Arctic – Technical Report 1, 2019.
- Virkkula, A., Ahlquist, N. C., Covert, D. S., Sheridan, P. J., Arnott, W. P., and Ogren, J. A.: A three-wavelength optical extinction cell for measuring aerosol light extinction and its application to determining light absorption coefficient, *Aerosol Sci. Tech.*, 39, 52–67, 535 <https://doi.org/10.1080/027868290901918>, 2005.

- Virkkula, A., Mäkelä, T., Yli-Tuomi, T., Hirsikko, A., Koponen, I. K., Hämeri, K., and Hillamo, R.: A simple procedure for correcting loading effects of aethalometer data, *J. Air Waste Manag. Assoc.*, 57, 1214–1222, <https://doi.org/10.3155/1047-3289.57.10.1214>, 2007.
- Virkkula, A.: Correction of the calibration of the 3-wavelength particle soot absorption photometer (3 λ PSAP), *Aerosol Sci. Tech.*, 44(8), 706–712, <https://doi.org/10.1080/02786826.2010.482110>, 2010.
- 540 Virkkula, A., Chi, X., Ding, A., Shen, Y., Nie, W., Qi, X., Zheng, L., Huang, X., Xie, Y., Wang, J., Petäjä, T., and Kulmala, M.: On the interpretation of the loading correction of the aethalometer, *Atmos. Meas. Tech.*, 8, 4415–4427, <https://doi.org/10.5194/amt-8-4415-2015>, 2015.
- Weingartner, E., Saathof, H., Schnaiter, M., Streit, N., Bitnar, B., and Baltensperger, U.: Absorption of light by soot particles: determination of the absorption coefficient by means of aethalometers, *J. Aerosol Sci.*, 34, 1445–1463, [https://doi.org/10.1016/S0021-8502\(03\)00359-8](https://doi.org/10.1016/S0021-8502(03)00359-8),
545 2003.
- Werle, P., Mücke, R., and Slemr, F.: The limits of signal averaging in atmospheric trace-gas monitoring by tunablediode-laser absorption spectroscopy (TDLAS). *Appl. Phys. B*, 57, 131–139, 1993.

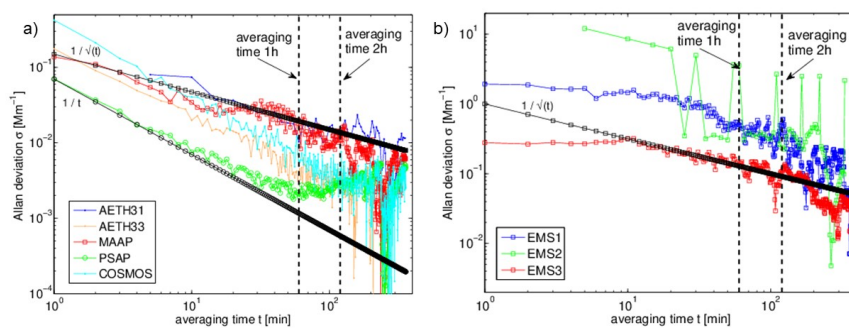


Figure 1. Allan deviation of aerosol absorption $\sigma_{AP,637nm}$ measured with a) the filter-based instruments and with b) the EMS technique. Averaging times between 1min and 6h are shown in x-axis. The black lines with slope -0.5 in a) and b) demonstrate white noise and in a) noise with slope -1.0 is added to guide the eye due to better fit with some instruments. Averaging times until 1h (marked with black dash line) improve signal-to-noise in all instruments but averaging 2h or more (marked with the second black dashed line) does not always lead to improvement.

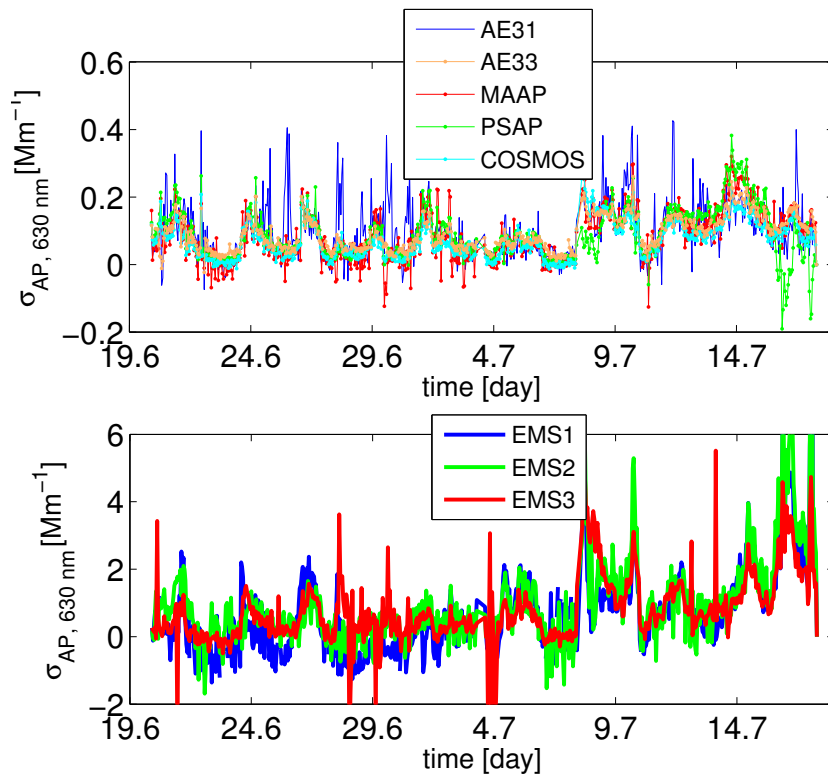


Figure 2. Hourly averaged absorption coefficient at $\lambda=630$ nm during the whole campaign period measured with the filter-based instruments (upper panel) and with the EMS-technique (lower panel).

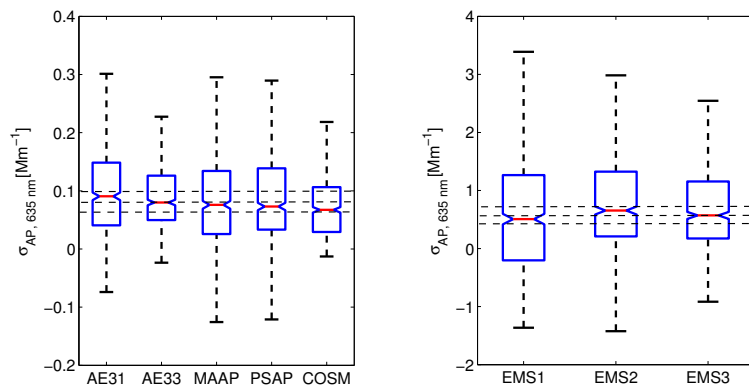


Figure 3. The vertical black lines show the range of 1h-averaged absorption coefficient values measured with the eight different techniques labeled in the x-axis. The red lines show the medians and the blue boxes the 25th and 75th percentiles. The horizontal dotted black lines present the overall medians $\pm 25\%$.

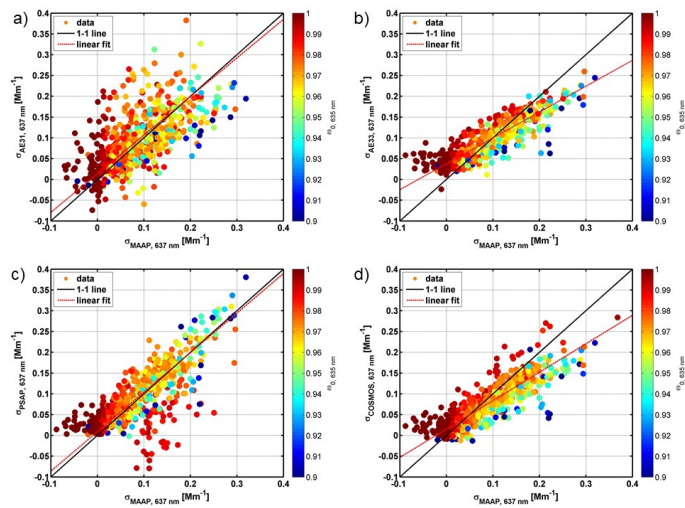


Figure 4. Bi-variate correlation of the 1h-averaged absorption coefficient measured by MAAP (x-axis) and by a) AE31, b) AE33, c) PSAP, and d) COSMOS at 637 nm. For each data value also 1h-averaged $\omega_{0,635 \text{ nm}}$ is presented as color. The corresponding correlation coefficients, their standard errors and the R^2 -statistics are presented in Table 4.

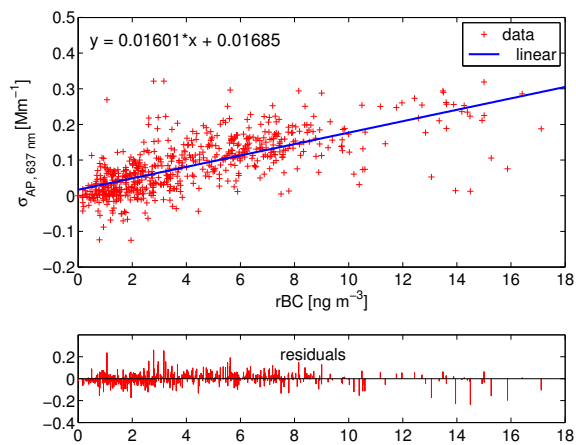


Figure 5. The absorption coefficient measured with MAAP as a function of the rBC concentration measured with SP2. The linear regression slope provides the corresponding mass absorption cross-section ($\text{MAC} = 16.0 \text{ m}^2 \text{ g}^{-1}$) value for MAAP and the lower panel presents the residuals of the correlation.

Table 1. The campaign instrumentation presented in columns: (1) instrument abbreviation, (2) variable measured (scattering = sca; extinction = ext; refractory Black Carbon = rBC; equivalent Black Carbon = eBC; particle number concentration = PN), (3) measurement time resolution, (4) flow rate, (5) instrument inlet (cut-size 10 μm = PM10 or Total inlet = TOT), and (6) lower detection limit based on manufacturer info.

| Instrument | Variable | Time res [s] | Volumetric Flow [LPM] | Inlet | Lower det limit [Mm^{-1}] |
|--------------|----------|--------------|-----------------------|-------|--------------------------------------|
| AE31 | eBC | 300 | 4.5 | TOT | <2.22 |
| AE33 | eBC | 60 | 5.8 | PM10 | <0.05 (1h) |
| MAAP | eBC | 60 | 8.0 | PM10 | <0.13 (30-min) |
| PSAP | eBC | 1 | 1.0 | PM10 | <0.1 (1-min) |
| COSMOS | rBC | 60 | 0.7 | PM10 | |
| SP2 | rBC | 1 | 0.1 | TOT | |
| CAPSex | ext | 5 | 0.8 | PM10 | <0.5 (1-min) |
| CAPSssa | ext | 1 | 0.9 | PM10 | <0.5 (1-min) |
| NEPH AUR4 | sca | 10 | 5.8 (via AE33) | PM10 | <0.3 (1-min) |
| NEPH TSI3563 | sca | 300 | 8.0 (via MAAP) | PM10 | <0.1 (30s) |

Table 2. The Allan deviation σ of absorption coefficient $\sigma_{AP,637nm}$ measured with different methods between 1–2hs averaging time (average \pm standard deviation).

| Method | σ ave \pm std [Mm] ⁻¹ |
|------------------|---|
| AE31 | 0.014 \pm 0.004 |
| AE33 | 0.003 \pm 0.001 |
| MAAP | 0.012 \pm 0.003 |
| PSAP | 0.002 \pm 0.000 |
| COSMOS | 0.005 \pm 0.002 |
| EMS ₁ | 0.379 \pm 0.104 |
| EMS ₂ | 0.806 \pm 1.100 |
| EMS ₃ | 0.107 \pm 0.030 |

Table 3. Average \pm standard deviation and median absorption coefficient $\sigma_{AP,635nm}$ measured with different methods.

| Method | $\sigma_{AP,635nm}$ ave \pm std [Mm] ⁻¹ | $\sigma_{AP,635nm}$ median [Mm] ⁻¹ |
|------------------|--|---|
| AE31 | 0.101 \pm 0.082 | 0.091 |
| AE33 | 0.090 \pm 0.050 | 0.080 |
| MAAP | 0.085 \pm 0.074 | 0.076 |
| PSAP | 0.088 \pm 0.074 | 0.073 |
| COSMOS | 0.073 \pm 0.054 | 0.067 |
| EMS ₁ | 0.709 \pm 1.312 | 0.507 |
| EMS ₂ | 0.952 \pm 1.303 | 0.654 |
| EMS ₃ | 0.785 \pm 1.015 | 0.570 |

Table 4. Linear regression statistics (correlation coefficients and standard error, SE) and R^2 -values for 1h-average absorption coefficient measured with filter-based instruments $y=m+bx$, where $x=MAAP$ and $y=AE31, AE33, PSAP$ or $COSMOS$. All presented correlations are statistically highly significant ($p<0.001$) and calculated at $\lambda = 637\text{nm}$.

| Instrument | slope = m (SE) | offset = b (SE) | R^2 |
|------------|----------------|-----------------|-------|
| AE31 | 0.93 (0.035) | 0.01 (0.004) | 0.65 |
| AE33 | 0.62 (0.014) | 0.04 (0.002) | 0.87 |
| PSAP | 0.95 (0.027) | 0.01 (0.003) | 0.78 |
| COSMOS | 0.68 (0.016) | 0.02 (0.002) | 0.85 |

Appendix A: Symbols and abbreviations

Table A1. Summary of symbols and abbreviations frequently used in the manuscript text.

| Symbol | Explanation |
|-------------------------|--|
| λ | Wavelength of light. |
| $\sigma_{SP,\lambda}$ | Scattering coefficient at wavelength λ . |
| $\sigma_{AP,\lambda}$ | Absorption coefficient at wavelength λ . |
| $\sigma_{EP,\lambda}$ | Extinction coefficient at wavelength λ . |
| $\sigma_{0,\lambda}$ | Absorption coefficient at wavelength λ as directly reported by instrument. |
| $\sigma_{INST,\lambda}$ | Absorption coefficient at wavelength λ after corrections measured with INST. |
| INST | Abbreviation of the absorption measurement instrument (see section 2 Methodology for a complete list of instruments used). |
| $\omega_{0,\lambda}$ | Single-scattering albedo at wavelength λ . |
| $\alpha_{SP,\lambda}$ | Ångström exponent of scattering at wavelength λ . |
| $\alpha_{AP,\lambda}$ | Ångström exponent of absorption at wavelength λ . |
| EMS _n | Extinction minus scattering technique to measure absorption, where n = 1, 2 or 3, referring to a pair of instruments used (see section 2 Methodology for details). |